15. Boyd E, Buchanan WW, Lennox B. Damage to chromosomes by therapeutic doses of radioiodine. *Lancet* 1961;1:977–978.
16. Baugnet-Mahieu L, Lemaire M, Leonard ED, et al. Chromosome aberrations after treatment with radioactive iodine for thyroid cancer. *Radiat Res* 1994;40:429–431.
17. Ottesen J. On age of human white cells in peripheral blood. *Acta Physiol Scand* 1954;32:75–93.
18. Norman A, Sasaki MS, Ottoman RE, Fingerhut AG. Lymphocyte lifetime in women. *Science* 1965;147:745.
19. Gutierrez S, Corbonell E, Galofrea P, et al. A cytogenic follow-up study of thyroid cancer patients treated with I-131. *Cancer* [Letters] 1995;91:199–204.
20. M'Kacher R, Legal JD, Schlumberger M, et al. Sequential biological dosimetry after a single treatment with iodine-131 for diffentiated thyroid carcinoma. *J Nucl Med* 1997;38:377–380.
21. Hall EJ. Repair of radiation damage and dose-rate effect. In: Hall EJ, ed. *Radiobiology for the radiologist*. Philadelphia: JB Lippincott, 1994:107–131.
22. M'Kacher R, Legal JD, Schlumberger M, et al. Biological dosimetry in patients treated with iodine-131 for differentiated thyroid carcinoma. *J Nucl Med* 1996;37:1860–1864.
23. Behr TM, Sharkey RM, Juweid MI, et al. Factors influencing the pharmacokinetics, dosimetry, and diagnostic accuracy of radioimmunodetection and radioimmunotherapy of carcinoembryonic antigen-expressing tumors. *Cancer Res* 1996;56:1805–1816.
24. Gunter HH, Junker D, Schober O, et al. Dosimetry of the hematopoietic system in radioiodine therapy of thyroid cancer. *Strahlentherapie und Onkologie* 1987;163:185–191.
25. McEwan AC. Absorbed doses in the marrow during I-131 therapy. *Br J Radiol* 1977;50:329–331.
26. Edmonds CJ, Smith T. The long-term hazards of the treatment of thyroid cancer. *Br J Radiol* 1986:59;45–51.
27. Brincker H, Hansen HS, Anderson AP. Induction of leukemia by I-131 treatment of thyroid carcinoma. *Br J Cancer* 1973:28;232–237.
28. Prosser JS, Moquet JE, Lloyd DC, Edwards AA. Radiation induction of micronuclei in human lymphocytes. *Mutat Res* 1988;199:37–45.
29. Kormos C, Koteles GJ. Micronuclei in X-irradiated human lymphocytes. *Mutat Res* 1988;199:31–35.

Glucose Metabolism in Human Malignant Gliomas Measured Quantitatively with PET, 1-[C-11]Glucose and FDG: Analysis of the FDG Lumped Constant

Alexander M. Spence, Mark Muzi, Michael M. Graham, Finbarr O'Sullivan, Kenneth A. Krohn, Jeanne M. Link, Thomas K. Lewellen, Barbara Lewellen, Scott D. Freeman, Mitchel S. Berger and George A. Ojemann

Departments of Neurology, Radiology, Statistics and Neurological Surgery, University of Washington School of Medicine, Seattle, Washington

Calculation of the glucose metabolic rate (MRGlc) in brain with PET and 2-[^{18}F]fluoro-2-deoxy-D-glucose (FDG) requires knowing the rate of uptake of FDG relative to glucose from plasma into metabolite pools in the tissue. The proportionality factor for this is the FDG lumped constant (LC_{FDG}), the ratio of the volumes of distribution of FDG and glucose multiplied by the hexokinase phosphorylation ratio for the two hexoses, $Km_{Glc}\cdot Vm_{FDG}/Km_{FDG}\cdot Vm_{Glc}$. MRGlc equals the FDG metabolic rate (MRFDG) divided by the LC_{FDG}, i.e., MRGlc = MRFDG/LC_{FDG} and LC_{FDG} = MRFDG/MRGlc. This investigation tested the hypothesis that LC_{FDG} is significantly higher in gliomas than it is in brain uninvolved with tumor. **Methods:** We imaged 40 patients with malignant gliomas with 1-[^{11}C]glucose followed by FDG. The metabolic rates MRGlc and MRFDG were estimated for glioma and contralateral brain regions of interest by an optimization program based on three-compartment, four-rate constant models for the two hexoses. **Results:** The LC_{FDG}, estimated as MRFDG/MRGlc, in gliomas was 1.40 ± 0.46 (mean ± s.d.; range = 0.72–3.10), whereas in non-tumor-bearing contralateral brain, it was 0.86 ± 0.14 (range = 0.61–1.21) ($p < 0.001$, glioma versus contralateral brain). **Conclusion:** These data strongly suggest that the glioma LC_{FDG} exceeds that of contralateral brain, that quantitation of the glioma MRGlc with FDG requires knowing the LC_{FDG} specific for the glioma and that the LC_{FDG} of normal brain is higher than previously reported estimates of about 0.50. 2-Fluoro-2-deoxy-D-glucose/PET studies in which glioma glucose metabolism is calculated by the autoradiographic approach with normal brain rate constants and LC_{FDG} will overestimate glioma MRGlc, to the extent that the glioma LC_{FDG} exceeds the normal brain LC_{FDG}. "Hot spots" visualized in FDG/PET studies of gliomas represent regions where MRGlc, LC_{FDG} or their product is higher in glioma than it is in uninvolved brain tissue.

Received Nov. 25, 1996; revision accepted Jun. 12, 1997.

For correspondence or reprints contact: Alexander M. Spence, MD, Department of Neurology, Box 356465, University of Washington, Seattle, WA 98195.

Key Words: lumped constant; glioma; glucose metabolism; brain neoplasm; PET

J Nucl Med 1998; 39:440–448

2-[^{18}F]fluoro-2-deoxyglucose (FDG) with PET is being used clinically in the management of malignant gliomas for grading, planning biopsies and distinguishing recurrent disease from radionecrosis (*1–9*). These studies have been based on simple visual assessment of FDG uptake (*1,9–11*), determination of the ratio of tumor FDG uptake to some normal brain reference region (*2,4,12,13*) or estimation of regional glucose metabolic rate (MRGlc) with FDG, based on the autoradiographic approach of Sokoloff et al. (*14*), applied with normal brain rate constants (*3,6,15–21*) or rate constants determined by dynamic imaging (*8,22,23*). The underpinning of these approaches is the fact that FDG, in a similar manner to glucose, is transported across the blood-brain barrier and phosphorylated by hexokinase (HK) to 2-fluoro-2-deoxy-D-glucose-6-phosphate, which accumulates in the tissue at a rate proportional to the rate of glucose utilization.

Because FDG and glucose differ in their rates of transport and phosphorylation and respective volumes of distribution in brain tissue, calculation of MRGlc from PET with FDG requires a proportionality constant, the FDG lumped constant (LC_{FDG}), in the operational equation (*14*). The LC_{FDG} represents the ratio of the metabolic rate of FDG (MRFDG) to MRGlc and, as such, is a complex constant that contains the Km and Vmax for FDG and glucose in the HK reaction, the ratios of the volumes of distribution of FDG and glucose (λ) and a ϕ term, assumed to be one, for the proportion of glucose which, once phosphorylated, is further metabolized. Mathematically:

$$LC_{FDG} = (\lambda/\phi)(Km_{Glc}\cdot Vm_{FDG}/Km_{FDG}\cdot Vm_{Glc}). \quad \text{Eq. 1}$$

From the operational equation for determining the MRGlc, MRGlc equals MRFDG divided by the LC_{FDG}, i.e.:

$$MRGlc = MRFDG/LC_{FDG} \quad \text{Eq. 2}$$

and

$$LC_{FDG} = MRFDG/MRGlc. \quad \text{Eq. 3}$$

This relationship shows that MRGlc and LC_{FDG} are inversely proportional to each other (*24*). The accuracy in measurement of MRGlc from PET with FDG depends on the accuracy of the LC_{FDG}; erroneous underestimation of the LC_{FDG} yields a correspondingly erroneous overestimation for MRGlc. Also, measurement of the ratio MRFDG/MRGlc provides an estimate of the LC_{FDG}. The LC_{FDG} in normal whole human brain has been estimated using dynamic PET by Phelps et al. (*20*) to be 0.42 and by Reivich et al. (*25*) to be 0.52. The LC_{FDG} heretofore has not been measured in human gliomas but has been assumed to be the same as normal brain (*3,6,8,15–19,21–23*).

We have shown by two separate biochemical approaches that the lumped constant of 2-[^{14}C]deoxyglucose (LC_{2DG}) of intracerebral transplants of the 36B-10 rat glioma exceeds that of normal brain by at least two-fold (*26,27*). Stemming from these results, this investigation examined the hypothesis that the LC_{FDG} is significantly higher in human malignant gliomas than it is in normal brain.

Our approach involved dynamic PET imaging of the kinetic behavior of 1-[^{11}C]glucose versus FDG in malignant gliomas and contralateral brain. We used compartmental mathematical models designed for the two tracers individually and calculated MRGlc and MRFDG for glioma and normal brain regions of interest (ROIs) and, from these, determined the regional LC_{FDG} as the ratio MRFDG/MRGlc. Estimating glioma glucose metabolism with both 1-[^{11}C]glucose and FDG has permitted us to explore the advantages of each tracer and the complementary information obtained from both used together.

MATERIALS AND METHODS

Patients

Forty patients, all with supratentorial malignant gliomas, were studied. Five cases were multicentric, and seven had bilateral tumors with involvement of the corpus callosum. There were 15 women (ages 24–68 yr; median = 45 yr) and 25 men (ages 28–66 yr; median = 52 yr). Thirty patients had glioblastoma multiforme (GBM), and 10 had anaplastic astrocytoma (AA). Seventeen patients were studied between the time of surgery for diagnosis and the start of radiotherapy. Twenty-three patients were studied at the time of recurrence after radiotherapy and/or chemotherapy. All patients signed informed consent.

Radiopharmaceutical Synthesis

2-[^{18}F]Fluoro-2-deoxy-D-glucose was synthesized by the method of Hamacher et al. (*28*). The FDG yield was typically 110 mCi 75 min after end of bombardment, which is a 45% decay-corrected radiochemical yield. The radiochemical and chemical purity of the product was measured by analytical high-performance liquid chromatography (HPLC) using an aminopropyl normal phase column (Alltech and Associates, Inc., Deerfield, IL) with a 93:7 (v/v) CH_3CN-to-H_2O mobile phase and refractive index and radioactivity detection of the effluent. Silica gel thin-layer chromatography with a 95:5 (v/v) CH_3CN-to-H_2O mobile phase was also used to assess radiochemical purity, which was consistently >99% for both methods. The measured specific activity of the FDG was >20 Ci/mmol at the end of synthesis.

The synthesis of 1-[^{11}C]glucose followed the method of Shiue and Wolf (*29,30*), as recently modified by Dence et al. (*31*). Typically, 1.7 Ci of [^{11}C]cyanide at the end of bombardment yielded 35–40 mCi of the 1-[^{11}C]glucose at the end of synthesis. The glucose was separated from mannose and any other impurities using an Aminex HPX-87P 30 cm × 7.8 mm HPLC column (Bio-Rad Laboratories, Hercules, CA) at 70°C and eluted with sterile water. The radiochemical and chemical purity of the product was measured by analytical HPLC using another Aminex HPX-87P column at 70°C, eluted with deionized water and with refractive index and radioactivity detection of the effluent.

PET Devices and Procedures

Two different PET systems were used over the course of this study. The first PET scans were obtained on a time-of-flight PETT Electronics SP-3000 device (*32–34*) containing four rings of BaF_2 detectors, 320 crystals in each ring. Axial collimation of photons in the tomograph allowed direct and cross-plane data to be collected, yielding seven image planes. This PET device acquired emission data in list mode format with timing markers that allowed selection of time binning of data after acquisition. The limiting resolution at the center of the field of view (FOV) was 5 mm in the transaxial plane and 7.5 or 11 mm in the axial plane. The interplane distance was 15 mm.

The second scanner was a General Electric (General Electric, Milwaukee, WI) Advance whole-body positron emission tomograph, providing 35 image planes of data over a 15-cm axial FOV (*35–37*). The tomograph included 18 rings of BGO detectors, with 672 crystals per ring. The system sensitivity in two-dimensional mode (axial septa in place) was 135 kcps/mCi/ml. The limiting transaxial resolution was 4.1 mm, with a slice thickness of 4 mm. The maximum counting rate obtainable with a head-sized phantom was over 2 M coincidence events/sec.

Imaging Procedure

Patients fasted for at least 9 hr before the scans. Before the PET scans, all patients had either x-ray CT or magnetic resonance imaging (MRI) scans, without and with contrast injections. From the scout images of these studies, axial image planes were selected for the PET scans to correspond to the planes containing the greatest tumor areas. After head immobilization was secured, patients were positioned in the tomograph. Alignment of the axial PET scan planes with those selected from the CT or MRI images was accomplished in the SP3000 by taking a lateral skull radiograph overlain with grid lines that corresponded to the planes of the tomograph. Patient and tomograph position and angulation were adjusted so that the PET tomograph planes corresponded to the desired CT or MRI axial planes. A system of laser beams then allowed advancing the patient's head into the tomograph to maintain the exact positioning in relation to the rings. Head positioning in the General Electric Advance tomograph was similar, except no scout films were used.

An attenuation scan was obtained with a rotating sector source of ^{68}Ge through the brain and tumor-containing region. While this was underway, an intravenous line was established for isotope injection, and a wrist radial artery line was inserted for plasma sampling for the isotope time-activity curve (TAC). The arterial line was connected to an automated blood sampler, which could be preprogrammed for the desired sampling sequence (*38*). Before scanning and isotope injection, a blood glucose level was drawn and analyzed by a Beckman Glucose Analyzer II. This was repeated several times after isotope injection.

After completion of the transmission/attenuation scans and placement of the vascular accesses, tomograph emission scan acquisition was started 1 min prior to injection of radioactive tracers. Calibration of the tomograph for μCi/cc was accomplished by imaging a 10-cm-diameter cylinder of known activity, as determined by a dose calibrator (Capintec, Ramsey, NJ), under

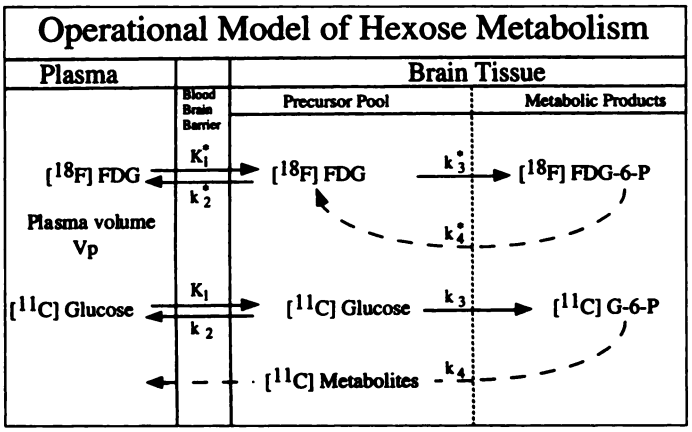

FIGURE 1. The models for glucose and FDG metabolism, showing the compartments and parameters.

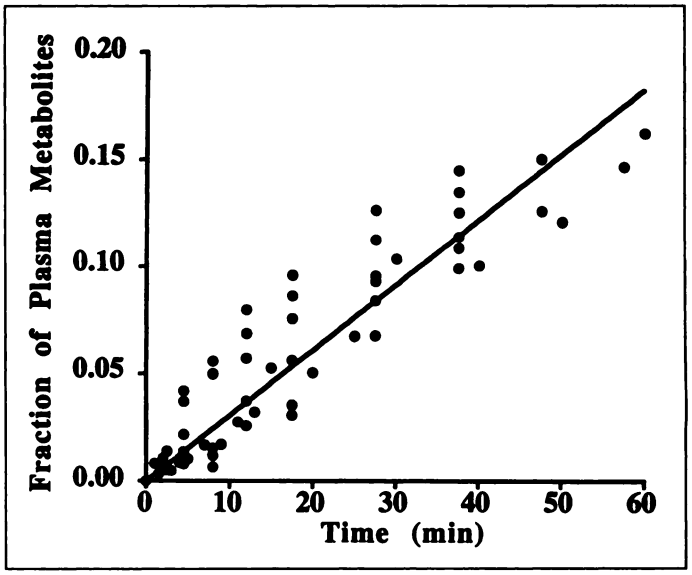

FIGURE 2. Plot of the ^{11}C-labeled metabolites of glucose in the plasma against the time after injection. Sixty minutes after injection, 18.3% of the ^{11}C in plasma is in metabolites. These data were used to correct the glucose plasma TACs and the plasma metabolite contribution to tissue activity in the tissue TACs.

similar conditions as those of the patient imaging protocol (30-cm FOV and 6-mm Hanning filter). For some studies, calibration was performed with the patient in the tomograph during the patient imaging procedure.

After 1 min of emission scan acquisition, 1-[^{11}C]glucose (typically 20 mCi) was injected intravenously over 1 or 2 min in 10 or 20 ml of sterile normal saline, respectively. After the 1-min preinjection scan, imaging data were collected and reconstructed in time bins as follows: 4 20-sec bins; 4 40-sec bins; 4 60-sec bins; 4 180-sec bins and 14 5-min bins.

Arterial blood was sampled at a frequency similar to that of the dynamic image acquisition. The 1-ml blood samples were centrifuged, and then 0.5 ml of plasma was pipetted and counted for total plasma radioactivity using a Cobra multichannel gamma counter (Packard Corp., Chicago, IL). Three 1-ml samples of the calibration cylinder were also obtained for well counting, which allowed us to express sample cpm/ml in terms of μCi/cc.

A FDG study followed each 1-[^{11}C]glucose study. Typically, we injected 7–10 mCi of FDG in 10 ml of normal saline over 1 or 2 min. Usually emission data were collected at frequency and timing identical to those of the glucose study after a similar 1-min preinjection scan. Blood was sampled and processed as described above.

Image Analysis

Regions of interest in the gliomas were selected to include the contrast enhancing volume and adjacent nonenhancing tumor, defined on MRI or CT images. They were drawn from the integrated FDG images while referencing MRI or CT images. Generally, ROIs were placed on the FDG uptake scans (30–60 min), and cysts and resection cavities were avoided. For nonenhancing tumors, the region of biopsy and T2 signal enhancing areas were selected conservatively. Contralateral brain regions included gray matter, white matter or both together. The model described below used the TACs from these regions expressed as μCi/cc, scaled using the conversion factor obtained from the calibration cylinder described above, and the blood input function in the same units of μCi/cc.

The contralateral brain or glioma ROI TACs were analyzed by means of the three-compartment models shown in Figure 1. The glucose model is similar to that described by Blomqvist et al. (*39*); the FDG model is that described by Phelps et al. (*20*), as a modification of Sokoloff's model for 2-deoxyglucose (*14*). The program incorporating these models used the plasma TACs as input functions. The tissue data were not decay-corrected because the models were formulated to account for this. Plasma data were corrected to time of sampling, not the time of injection. The [^{11}C]glucose plasma data were corrected for metabolites (CO_2 and lactate), assuming linear accumulation of metabolites, such that 18% of plasma activity at 60 min could be ascribed to metabolites in the same fashion as reported by Blomqvist et al. (*39*). It was further assumed that the metabolites remained in the vascular space and were not taken up into tissue.

We confirmed the accumulation rate of metabolites by analyzing plasma samples from patients during PET studies by column separation. Our data consisted of 58 points from seven patients, with 6–16 points per patient. The results are shown in Figure 2. The linear fit to the data, constrained to pass through the origin, had $R^2 = 0.86$, s.e.e. = 1.8% and a value of 18.3% at 60 min.

The predicted tissue TACs were calculated using numeric integration of the differential equations for each model. The tail of the [^{11}C]glucose activity was appropriately added to the FDG activity because the FDG was injected second. There were a total of 11 variable parameters: K1, k2, k3 and k4 for [^{11}C]glucose; K1, k2, k3 and k4 for FDG; a delay term to shift the tissue activity relative to the plasma curve for both tracers; and a blood volume term to account for activity in large blood vessels. An additional important constraint forced the K1/k2 ratios for both [^{11}C]glucose and FDG to be the same. This is based on the symmetry of glucose transport between blood and tissue, as shown by Gjedde and Diemer (*40*). The effect of this constraint, rather than to estimate K1 and k2 independently, is that the number of parameters is dropped by one and the accuracy of individual parameter estimates is improved. The "best-fitting" model to a given data set was achieved using an established nonlinear weighted least squares algorithm (*41*). The algorithm minimized the sums of the squares of the differences between the model output and the tissue data, weighted proportionally to the inverse square root of the count of each data point. With this optimization program, the rate constants were estimated for [^{11}C]glucose and FDG for ROI TACs obtained from contralateral whole brain, gray matter, white matter or malignant glioma tissue. The metabolic rate constant (defined as MR) for each hexose was calculated as:

$$MR = (K1 \cdot k3)/(k2 + k3). \qquad \text{Eq. 4}$$

LC_{FDG} was calculated from the ratio of the metabolic rates for the two hexoses, i.e., MRFDG/MRGlc.

TABLE 1
Kinetic Rate Constants, MRGlc, MRFDG and LC_{FDG} of Brain and Glioma Regions for the 59-Yr-Old Man Whose Images Are Illustrated in Figure 5

	Contralateral brain		Contralateral gray matter		Contralateral white matter		Glioma	
	Mean	s.d.	Mean	s.d.	Mean	s.d.	Mean	s.d.
1-[^{11}C] Glucose								
K1 (ml/g/min)	0.066	0.019	0.079	0.029	0.043	0.016	0.067	0.045
k2 (min^{-1})	0.173	0.134	0.202	0.187	0.122	0.146	0.237	0.219
k3 (min^{-1})	0.217	0.083	0.278	0.128	0.187	0.155	0.154	0.159
k4 (min^{-1})	0.010	0.004	0.011	0.005	0.009	0.007	0.014	0.011
FDG								
K1 (ml/g/min)	0.103	0.044	0.116	0.047	0.059	0.025	0.089	0.054
k2 (min^{-1})	0.252	0.164	0.254	0.183	0.149	0.129	0.269	0.205
k3 (min^{-1})	0.108	0.044	0.116	0.058	0.090	0.098	0.135	0.079
k4 (min^{-1})	0.011	0.007	0.011	0.011	0.013	0.012	0.015	0.018
MRGlc* (μmol/100 g/min)	21.8	5.9	26.0	7.2	14.1	4.6	12.4	6.2
MRFDG† (μmol/100 g/min)	18.2	5.1	21.2	6.0	12.3	4.5	16.2	6.7
$\frac{MRFDG}{MRGlc} = LC$	0.86	0.14	0.83	0.15	0.89	0.18	1.40	0.46

*$MRGlc = Cp \cdot K1 \cdot (k3/k2 + k3)$.
†$MRFDG = Cp \cdot K1_{FDG} \cdot (k3_{FDG}/k2_{FDG} + k3_{FDG})$.

Statistics

Student's paired t-test was used to compare LC_{FDG} in malignant glioma ROIs to LC_{FDG} in contralateral brain ROIs.

RESULTS

Sixteen patients were imaged with the SP3000 camera, and 24 were imaged with the General Electric Advance scanner. Table 1 shows the kinetic rate constants, MRGlc, MRFDG and LC_{FDG} for all cases. These results were derived from analysis of glioma or contralateral brain ROIs and parameter optimization, based on the three-compartment, four-parameter models. The mean LC_{FDG}, determined as MRFDG/MRGlc, was 0.86 ± 0.14 (mean ± s.d.) in contralateral whole-brain regions, 0.83 ± 0.15 in gray matter and 0.89 ± 0.18 in white matter, whereas for glioma regions, it was 1.40 ± 0.46 ($p < 0.001$, glioma versus whole brain, gray matter or white matter). Figure 3 shows this and the spread of the data graphically for contralateral brain and glioma. Figure 4 is a histogram of the ratio of the LC_{FDG} for glioma to the LC_{FDG} of contralateral brain. In 37 of the 40 cases, the ratio was greater than unity. The mean LC_{FDG} for the 10 AA patients was 1.23 ± 0.35, whereas for the 30 GBM patients, it was 1.47 ± 0.48; this difference was not significant by the Student's t-test. When the rate constants MRGlc, MRFDG and LC_{FDG} for glioma, contralateral brain, gray matter or white matter determined with the SP3000 tomograph were compared to those determined with the Advance tomograph, there were no significant differences.

To exemplify the results, the case of a 59-yr-old man with a deep right hemisphere GBM is presented. Table 2 shows the data generated by optimization from seven planes. For his glioma, the MRGlc was 12.3 μmol/100 g/min, the MRFDG was 22.2 and the LC_{FDG} was 1.81. For his contralateral brain, MRGlc was 31.4, MRFDG was 21.0 and the LC_{FDG} was 0.67. Figure 5 shows his 1-[^{11}C]glucose, FDG and gadolinium-enhanced magnetic resonance images, all from the same plane. These PET scans were performed after surgery but before radiotherapy. The 1-[^{11}C]glucose image was integrated from 5 to 25 min, and the FDG image was integrated from 30 to 60 min. The integrated 1-[^{11}C]glucose image suggests that the glioma was not metabolically more active than cortex, whereas the FDG-integrated image suggests that it was.

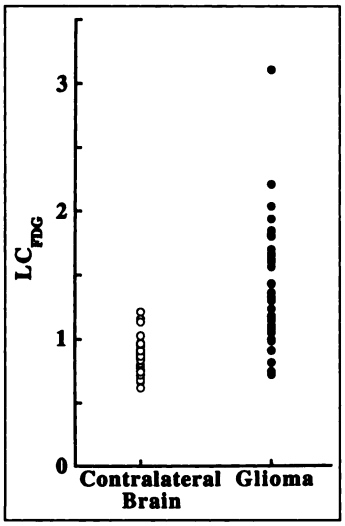

FIGURE 3. Scatter graphs showing the distribution of the LC_{FDG} in contralateral brain and the gliomas. There is considerably more spread in the glioma data compared to contralateral brain.

TABLE 2
Metabolic Rates of Glucose and Fluoro-2-deoxy-D-glucose and Fluoro-2-deoxy-D-glucose Lumped Constant of Contralateral Brain and Glioma for a 59-Yr-Old Man (Fig. 5)

	Contralateral brain	Glioma
1-[^{11}C] Glucose		
K1 (ml/g/min)	0.083	0.081
k2 (min^{-1})	0.230	0.178
k3 (min^{-1})	0.218	0.043
k4 (min^{-1})	0.015	0.009
FDG		
K1 (ml/g/min)	0.117	0.067
k2 (min^{-1})	0.324	0.146
k3 (min^{-1})	0.097	0.110
k4 (min^{-1})	0.007	0.005
MRGlc (μmol/100 g/min)	31.4	12.3
MRFDG (μmol/100 g/min)	21.0	22.2
$\frac{MRFDG}{MRGlc} = LC$	0.67	1.81

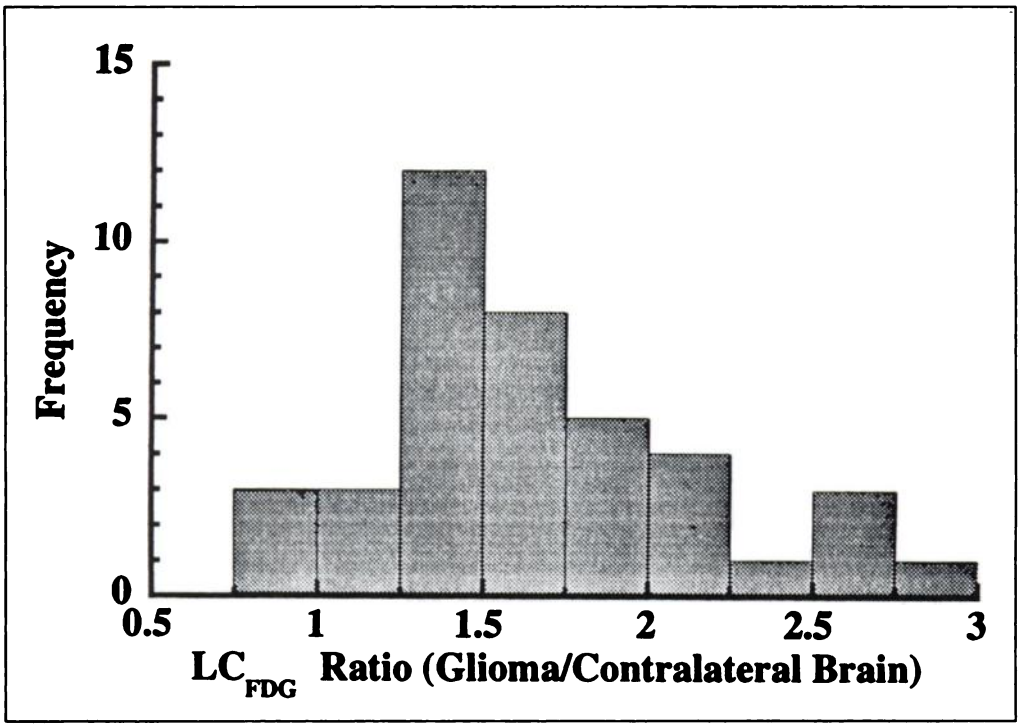

FIGURE 4. Frequency histogram of the ratios of the LC_{FDG} values for glioma to the LC_{FDG} values of contralateral brain. The median is 1.56.

DISCUSSION

This investigation was undertaken to improve our understanding of regional MRGlc in human malignant gliomas. To achieve this with FDG required clarification of the question of whether glioma and normal brain tissue share the same LC_{FDG} and determination of the MRGlc with glucose alone to obviate the need for assuming a value for LC_{FDG}. Our data confirm that the LC_{FDG} is higher in malignant gliomas than it is in contralateral brain and that it is variable among patients.

These human results completely agree with the explicit biochemical measurements of the LC_{2DG} in a rat glioma model and normal rat brain that were reported previously (*26,27*). Based on the method of Crane et al. (*42*) for determining the hexose utilization index as an estimate of the LC_{2DG} (*27*), we found that the hexose utilization index in glioma implants exceeded that of uninvolved contralateral brain by 1.5–1.7 times. Measuring the volumes of distribution of glucose and 2-[^{14}C]deoxyglucose and the ratio $K1_{2DG}/K1_{Glc}$ (*43*) further allowed us to derive the LC_{2DG} for tumor (LC_T) relative to that for contralateral brain (LC_N). LC_T was 2.1 times higher (*27*). We also measured the HK Km and Vmax values for 2-[^{14}C]deoxyglucose and glucose in normal rat brain and in intracerebral and subcutaneous 36B-10 glioma grafts (*26*). The phosphorylation ratio $Km_{Glc}\cdot Vm_{2DG}/Km_{2DG}\cdot Vm_{Glc}$ was two-fold higher in glioma than it was in normal brain. These findings led to an explicit calculation of the glioma LC_{2DG} when they were combined with the measured volume of distribution values (λ) in the formula: $LC_{2DG} = (\lambda/\phi)(Km_{Glc}\cdot Vm_{2DG}/Km_{2DG}\cdot Vm_{Glc})$. Assuming $\phi = 1$ (*14*), this approach yielded a LC_{2DG} of 0.517 ± 0.051 (mean ± s.d.) in normal rat brain and 1.168 ± 0.171 in intracerebral 36B-10 implants. The ratio LC_T/LC_N was 2.26 ± 0.73. These observations from the rat glioma model concordantly suggested that measurement of brain tumor MRGlc using FDG and a normal brain LC would significantly overestimate the true tumor MRGlc by as high as two-fold (100%).

Measurements of malignant glioma MRGlc with PET and 1-[^{11}C]glucose have not been rigorously attempted before, but such studies for normal human brain have been reported by Blomqvist et al. (*39*). They performed PET scans on normal human volunteers after administering 1-[^{11}C]glucose and additionally sampled jugular venous blood to allow measurements

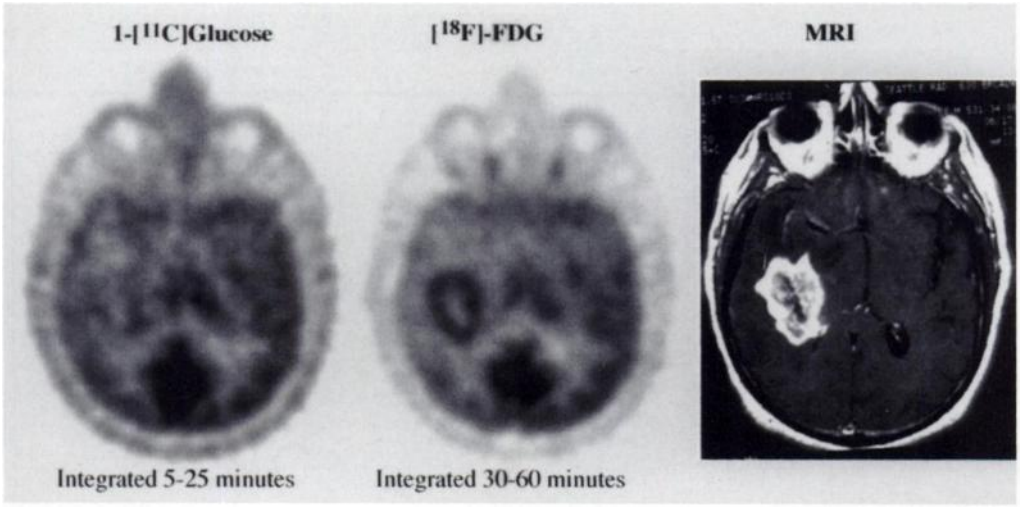

FIGURE 5. Images from a 59-yr-old man with a deep right hemisphere GBM, all from the same plane.

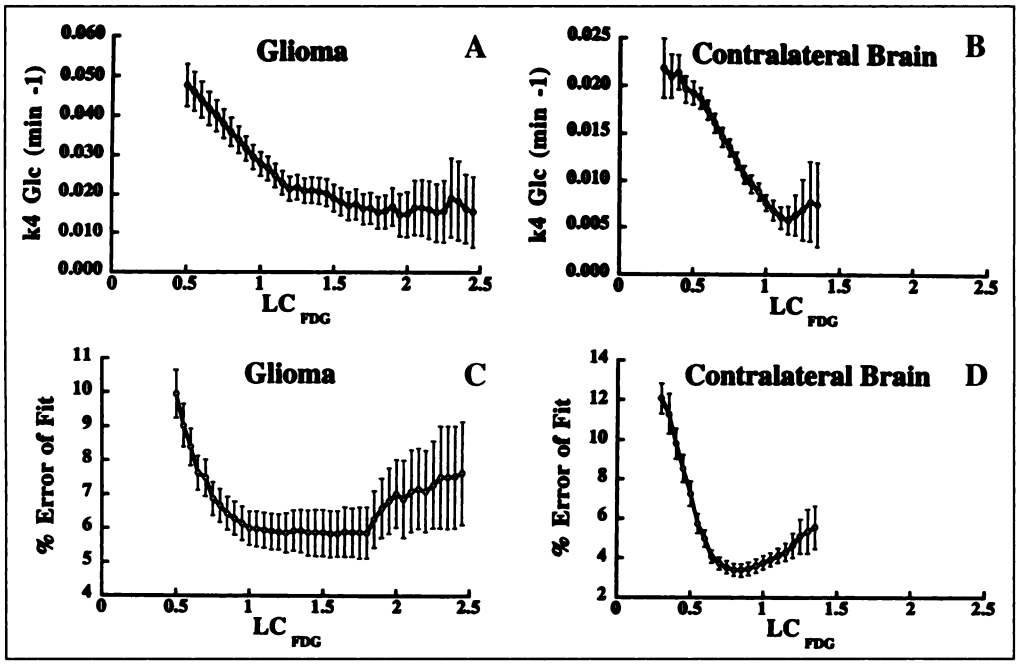

FIGURE 6. (A) Plot of $k4_{Glc}$ versus a range of values for the LC_{FDG} from the glioma dataset. As the LC_{FDG} is successively lowered, there is a rise in the $k4_{Glc}$. Our estimate of the LC_{FDG} of 1.40 corresponds to $k4_{Glc}$ of about 0.017. If LC_{FDG} were the same in glioma as contralateral brain (~0.85), $k4_{Glc}$ would be estimated to be two times higher (~0.034). Error bars are s.e. The minima of the curves do not exactly match the mean estimates of LC_{FDG} or $k4_{Glc}$ (Table 1) because of the way the curves average together. Because the curves are very nonlinear, the minimum of the average curve does not necessarily match the average of the minima for individual curves. (B) Plot of $k4_{Glc}$ versus a range of values for the LC_{FDG} from the contralateral brain data set. As the LC_{FDG} is successively lowered, there is also a rise in the $k4_{Glc}$. Our estimate of the LC_{FDG} of 0.86 corresponds to $k4_{Glc}$ of 0.010. (C) Plot of the percentage error in the fit versus a range of values of the LC_{FDG} from the glioma data set. The best fit for the LC_{FDG} in the gliomas is for the LC_{FDG} between 1.15 and 1.80, corresponding to $k4_{Glc}$ of 0.015–0.020 (A). (D) Plot of the percentage error in the fit versus a range of values of the LC_{FDG} from the contralateral brain data set. The best fit for the LC_{FDG} in the contralateral brain is for the LC_{FDG} of 0.80, corresponding to $k4_{Glc}$ of about 0.010 (B).

of arteriovenous differences for unlabeled O_2, glucose, CO_2 and acidic glucose metabolites. They collected their data over 24 min and analyzed them with a three-compartment model. Blood flow was measured with [^{11}C]fluoromethane. After injection of 1-[^{11}C]glucose, plasma metabolites, including CO_2, increased to approximately 10% of plasma activity over 24 min. Correction for CO_2 and metabolite loss from tissue and for effects of CO_2 and metabolites on plasma ^{11}C TACs yielded a 12% increase in estimated MRGlc from 23.6 ± 0.8 μmol/100 g/min to 26.4 ± 0.8 μmol/100 g/min. This was not significantly different from the MRGlc of 28.3 ± 4.3 μmol/100 g/min measured by the Fick principle. Thus, the error in measurement of normal brain MRGlc from using PET with 1-[^{11}C]glucose without accounting for CO_2 and metabolites in the tissue and plasma TACs was only about 17%. This is noteworthy in view of the fact that an error as high as 70%–100% in estimation of absolute MRGlc in malignant gliomas would result from a FDG/PET study if the glioma lumped constant was as high as that from our previous rat data (*26,27*) and current human glioma data suggest that it is.

The conclusion from this study, that the LC_{FDG} is elevated in gliomas, depends on the validity of the two kinetic models used. The deoxyglucose model (including FDG) has been used for two decades and has been carefully examined by numerous investigators. It has been used with apparent success in several different tissue types (*44–47*). Herholz et al. (*48*) has examined the validity of FDG in brain tumors and found the model to be valid, except for significant concern regarding the value of the lumped constant. The only significant critique of the model is that a few metabolites appear in the plasma for relatively long periods after injection (*46,49–52*). The levels of these metabolites during the first 60–90 min after injection are very low and have virtually no effect on the modeling results.

The validity of the glucose model is not as well established. Metabolism of glucose continues past glucose-6-phosphate, with production and release of diffusible metabolites such as lactate and CO_2. The approach used in this study takes circulating metabolites into account. Metabolites build up linearly in the plasma, reaching 18% at 60 min. It is assumed that the metabolites do not enter tissue to any significant extent but do contribute to activity in the blood volume of the tissue. This assumption may not be entirely correct for tumors because of the greater permeability between plasma and tissue than in normal brain. However, because the fraction of activity in plasma metabolites is low early in the study, when [^{11}C]glucose levels are high, the metabolites make little difference to the plasma TAC and, thus, make little difference in the tissue TAC.

We have considered the possibility that the difference in behavior between FDG and glucose that we detect in tumors is due to glycolysis with increased production of lactate. If this were the case, the k4 for glucose ($k4_{Glc}$) should be markedly elevated in the gliomas. We observed that $k4_{Glc}$ for the gliomas was 0.014 ± 0.011 and for contralateral brain was 0.010 ± 0.004. We looked at the possibility that $k4_{Glc}$ of gliomas is actually higher by fixing the LC_{FDG} at lower values (by fixing the ratios between the FDG and glucose parameters) and floating the remaining parameters in the optimization. Figure 6A and B, show the trade-off between $k4_{Glc}$ and LC_{FDG} in the gliomas and contralateral brain ROIs, respectively. When LC_{FDG} is lower, the $k4_{Glc}$ is higher. However, as LC_{FDG} is lowered, the fit of the model output to the observed tissue data becomes progressively worse in both the gliomas and contralateral brain. Figure 6C shows a plot of the percentage error in the fit versus LC_{FDG} in the glioma dataset. Because LC_{FDG} is constrained to lower values, the percentage error in the fit becomes progressively worse. Examination of the plots for both glioma and contralateral brain ROIs (Figure 6C and D, respectively) shows that the best fits (lowest percentage errors) are

obtained with much higher values of LC_{FDG} for gliomas than for normal tissue. Although the percentage error in the fit versus LC_{FDG} is relatively flat in the area of the minima, the curve for gliomas is generally to the right (higher values of LC_{FDG}) of the curve for contralateral brain tissue.

This modeling analysis supports the concept that the LC_{FDG} is higher for tumor than for normal tissue. It does not address the possibility that the glucose model itself could be wrong. Certainly, the model is a simplified approximation of the kinetics of glucose. There is likely to be a significant delay for some of the loss of ^{11}C label from tissue because the C1 carbon of glucose is not lost to CO_2 until two and a half turns of the tricarboxylic acid cycle and the pentose shunt fraction is likely to be low (*53*). Although glycolysis with production of lactate is likely to be high in gliomas, loss from the tissue may not be a rapid process because the pool size for lactate may be substantial (*54*). Also, some of the ^{11}C-labeled metabolites will be retained in the tissue permanently and will not be available for loss. We examined these possibilities by testing the model with two additional rate constants. k5 was a second loss rate constant that began only after a delay. k6 was a rate constant for activity that was permanently retained in the tissue. When these parameters were allowed to float during optimization, they always went to zero, indicating they were unnecessary for describing the kinetics of 1-[^{11}C]glucose.

Another assumption included in the model analysis is that the K1/k2 ratio is the same for both 1-[^{11}C]glucose and FDG. This is based on the observation by Gjedde and Diemer (*40*) that hexose transport between plasma and brain is symmetric, which implies that the ratio of K1 to k2 should be the same for all hexoses. We tested this hypothesis by computing the K1/k2 ratio for all brain and tumor region TACs without the K1/k2 constraint. We found the median value of the ratio of the K1/k2 ratios ($K1_{Glc}/k2_{Glc}/K1_{FDG}/k2_{FDG}$) was 1.13, with no significant difference between tumor and normal regions. This outcome is consistent with the K1/k2 ratios being the same for the two hexoses. We also examined the effect of the K1/k2 constraint on the goodness of fit of the model to the data. Addition of this constraint resulted in a small but statistically significant worsening in the fit. We interpret this to indicate that the glucose model is not entirely correct and that addition of an extra parameter provides additional flexibility, resulting in a better fit. We have examined the overall outcomes using both models and have found only minimal differences that have no effect on the conclusions presented in this paper. We chose to use the model with the K1/k2 constraint because it is more biochemically realistic and yields physiologically plausible parameter estimates more consistently than does the unconstrained model.

If breakdown of glucose to lactate and substantial loss of lactate to plasma took place within seconds, the glucose model could fail to account for glycolysis. Changing the model would make little difference with the current data collection scheme because 1-[^{11}C]glucose is injected over 1 or 2 min, and images are collected at 15-sec to 1-min intervals early in the studies. A distributed model (*55*) along with bolus injection and more rapid data acquisition would be necessary to define such rapid parameters. However, it is unlikely that the rate constants are so high that we cannot observe them. K1 is a combination of blood flow and delivery. It cannot be higher than blood flow, i.e., 0.3–1.0 ml/g/min. The washout rate constant, k2, is also limited by blood flow and thus cannot exceed 1.0/min. The cerebral transport rate constant for lactate (~k4) has been measured in rats and is approximately 0.13/min in normal brain (*56*). Even if k3 were very high, the reasonable values of the other constants constrain the kinetics to rates that should be observable with our data collection approach. Thus, we doubt that glycolysis and loss of labeled lactate is happening so rapidly that we cannot detect it. The main support for the glucose model is that it yields values for MRGlc in normal brain that are consistent with those reported by Blomqvist et al. (*39*) from an extraction experiment.

The value of the lumped constant is largely determined by differences in the kinetics of HK for glucose and deoxyglucose. It is likely that the increased value of the lumped constant in gliomas is due to different HK kinetics for the two hexoses compared to normal brain. The elevated LC_{FDG} in gliomas is probably not due to an increase of HK activity because recent data show that these tumors do not have higher HK activity than normal brain (*57,58*).

Of interest are several emerging concepts relevant to HK in brain and gliomas. In normal brain, the predominant isozyme of HK is HKI, which is bound to the outer mitochondrial membrane where it has a higher affinity for glucose than does unbound HKI (*59–63*). In gliomas, there is a shift to a greater proportion of the isozyme, HKII, relative to HKI, similar to reports in other tumor systems (*59,64–67*), and HKII does not associate with mitochondria as avidly as does HKI (*61*). HKII demonstrates a higher Km (less affinity) for glucose (*65,68–71*) as well as for deoxyglucose (*26,69*) than does HKI. Gliomas are mainly astrocytic, and in normal glia, HK is mainly cytoplasmic (*63,72*). Lastly, rat myocardial HKII shows an 8.5 fold increase in affinity for FDG (lower Km_{FDG}) in the cytosolic state compared to the mitochondrially bound state (*73*).

From these points follows a plausible explanation for the increase in the LC_{FDG} in malignant gliomas. The equation $LC_{FDG} = (\lambda/\phi)(Km_{Glc} \cdot Vm_{FDG}/Km_{FDG} \cdot Vm_{Glc})$ shows that the LC_{FDG} is proportional to Km_{Glc}/Km_{FDG}. In malignant gliomas, a shift of HKI from bound to unbound configuration would raise Km_{Glc}, whereas a higher proportion of HKII that is not mitochondrially bound would lower Km_{FDG}. Together, these changes would raise Km_{Glc}/Km_{FDG} and LC_{FDG}, all consistent with the tumors having less bound HK, less overall HK activity and a greater proportion of HKII. These ideas, drawn mainly from rat investigations, need to be confirmed with glucose, FDG and a human source of the HK isozymes. The Michaelis–Menten kinetics of human HKI and HKII, mitochondrial and cytosolic, need to be determined for both hexoses, as do the proportion of HKI and HKII isozymes in normal brain and glioma tissue, and the proportion of bound versus free isozymes. The void in our understanding of the HK reaction in human brain and gliomas and in FDG/PET imaging of gliomas in particular is that the kinetics of human HKI and HKII expecially for glucose and FDG have not been adequately worked out.

The lumped constants we have determined in the contralateral brain are higher than previously reported values for normal brain. Phelps et al. (*20*) found it to be 0.42, whereas Reivich et al. (*25*) found it to be 0.52. There are several potential explanations for this difference. Fluorodeoxymannose contamination of FDG in previous studies would lead to an underestimation of the LC_{FDG} by approximately 10% (*25*) or higher (*74*). Omission of the k4 for FDG in the models lowers the LC_{FDG} in brain by roughly 10% (*25*) (*unpublished observations*). Additionally, estimation of the LC_{FDG} can be influenced by the proportion of gray and white matter included in the examined region of brain and the amount of partial volume effects of cerebrospinal fluid spaces on brain tissue. By a different approach than ours, Lammertsma et al. (*75*) assessed the LC_{FDG} by measuring oxygen and FDG uptake in whole brain or cortex in three normal subjects. They found values of

LC_{FDG} between 0.57 and 0.77, depending on the analytical technique used. To clarify this further, we are conducting studies of brain LC_{FDG} in non-tumor-bearing normal volunteers by the approach we have reported above.

The implications of this work for nuclear medicine and neurooncology are that FDG/PET studies in which glioma glucose metabolism is calculated by the autoradiographic approach with normal brain rate constants and LC_{FDG} will overestimate glioma MRGlc to the extent that the glioma LC_{FDG} exceeds the normal brain LC_{FDG} (*3,6,8,14–23*). In the visual "hot spot" imaging approach, the hot spots represent regions where MRGlc, LC_{FDG} or their product are higher in glioma than they are in uninvolved brain tissue (*1,9–11*).

Our findings do not detract from the position taken by The Therapeutics and Technology Assessment Subcommittee of the American Academy of Neurology, which has stated that "cerebral glucose metabolic studies are extremely useful in the management of brain neoplasms" (*76*). The FDG/PET technique is useful for grading tumors and estimating prognosis (*3*) and in presurgical planning for biopsies (*77*). Also, FDG/PET has the capacity to distinguish radionecrosis from recurrent glioma (*9,10*). From numerous studies, the evidence suggests that increased FDG uptake indicates malignancy, early recurrence or poor response to therapy. Despite these advances, none of the studies has compared visual imaging, the autoradiographic approach with FDG or calculated ratios to accurate metabolic imaging in gliomas based on an understanding of the glioma lumped constant.

The problems inherent with visual imaging and deriving ratios of glioma regions relative to a normal brain reference region are:

1. Most patients are on anticonvulsants that can lower cortical glucose metabolism by 7%–30% (*78*);
2. Diaschisis effects can lower glucose metabolism in non-tumor-bearing cerebral and cerebellar regions (*15,79–82*);
3. There is relative lack of control over the patient's cortical activity during scanning as influenced by sensory stimuli such as pain, state of arousal, motor activity, thinking, day dreaming, anxiety and so on.

Strong statements to the effect that visual interpretation is better than accurate quantitation are embedded in the literature (*1,10,11,83*). Although these claims may turn out to be correct for clinical decision making, they are clearly conjectural, i.e., not based on a rigorous comparison of visual imaging versus accurate quantitation, because the latter has never heretofore been performed with a full and accurate understanding of the proportionality of FDG relative to glucose uptake in neoplastic tissue.

Lastly, studies based on FDG alone, with or without the LC_{FDG} for tumor tissue, cannot answer some important and practical questions, such as whether therapy lowers or raises the absolute MRGlc, changes transport or the HK reaction or changes the rate of glycolysis relative to oxidative metabolism. Further investigations with 1-[^{11}C]glucose combined with FDG are underway to explore these questions.

CONCLUSION

This study of 40 patients has yielded evidence that the LC_{FDG} in malignant gliomas is substantially elevated and varies widely from tumor to tumor. Dynamic FDG/PET studies in which glioma glucose metabolism is calculated by the autoradiographic approach with the normal brain LC_{FDG} will overestimate the glioma glucose metabolic rate to the extent that the glioma LC_{FDG} exceeds the normal brain LC_{FDG}. This may apply to nonbrain malignancies as well. Additionally, contralateral cerebral regions in glioma-bearing patients demonstrated higher LC_{FDG} values than reported in prior studies of the normal brain, suggesting that the normal brain LC_{FDG} may be higher than the generally accepted value.

ACKNOWLEDGMENTS

This work was supported by National Institutes of Health Grant CA42045.

REFERENCES

1. Alavi JB, Alavi A, Chawluk J, et al. Positron emission tomography in patients with glioma: a predictor of prognosis. *Cancer* 1988;62:1074–1078.
2. Coleman RE, Hoffman JM, Hanson MW, Sostman HD, Schold SCJ. Clinical application of PET for the evaluation of brain tumors. *J Nucl Med* 1991;32:616–622.
3. Di Chiro G. Positron emission tomography using [^{18}F]fluorodeoxyglucose in brain tumors: a powerful diagnostic and prognostic tool. *Invest Radiol* 1987;22:360–371.
4. Glantz MJ, Hoffman JM, Coleman RE, et al. Identification of early recurrence of primary central nervous system tumors by [^{18}F]fluorodeoxyglucose positron emission tomography. *Ann Neurol* 1991;29:347–355.
5. Herholz K, Pietrzyk U, Voges J, et al. Correlation of glucose consumption and tumor cell density in astrocytomas. A stereotactic PET study. *J Neurosurg* 1993;79:853–858.
6. Ishikawa M, Kikuchi H, Miyatake S, Oda Y, Yonekura Y, Nishizawa S. Glucose consumption in recurrent gliomas. *Neurosurgery* 1993;33:28–33.
7. Kim EE, Chung SK, Haynie TP, et al. Differentiation of residual or recurrent tumors from post-treatment changes with F-18 FDG PET. *Radiographics* 1992;12:269–279.
8. Tyler JL, Diksic M, Villemure JG, et al. Metabolic and hemodynamic evaluation of gliomas using positron emission tomography. *J Nucl Med* 1987;28:1123–1133.
9. Valk PE, Budinger TF, Levin VA, Silver P, Gutin PH, Doyle WK. PET of malignant cerebral tumors after interstitial brachytherapy. *J Neurosurg* 1988;69:830–838.
10. Doyle WK, Budinger TF, Valk PE, Levin VA, Gutin PH. Differentiation of cerebral radiation necrosis from tumor recurrence by [^{18}F]FDG and ^{82}Rb positron emission tomography. *J Comput Assist Tomogr* 1987;11:563–570.
11. Schifter T, Hoffman JM, Hanson MW, et al. Serial FDG-PET studies in the prediction of survival in patients with primary brain tumors. *J Comput Assist Tomogr* 1993;17:509–516.
12. McKusick KA, Fischman AJ, Hochberg FH, Alpert NM, Corriera JA, Strauss HW. TL-201 and F-18 deoxyglucose in detection of recurrent primary brain tumor [Abstract]. *J Nucl Med* 1991;32:955.
13. Schifter T, Hoffman JM, Hanson MW, et al. Serial FDG-PET studies in the management of primary CNS tumors [Abstract]. *J Nucl Med* 1991;32:932.
14. Sokoloff L, Reivich M, Kennedy C, et al. The [^{14}C]deoxyglucose method for the measurement of local cerebral glucose utilization: theory, procedure, and normal values in the conscious and anesthetized albino rat. *J Neurochem* 1977;28:897–916.
15. Di Chiro G, DeLaPaz RL, Brooks RA, et al. Glucose utilization of cerebral gliomas measured by [^{18}F]fluorodeoxyglucose and positron emission tomography. *Neurology* 1982;32:1323–1329.
16. Mineura K, Yasuda T, Kowada M, Ogawa T, Shishido F, Uemura K. Positron emission tomographic evaluation of radiochemotherapeutic effect on regional cerebral hemocirculation and metabolism in patients with gliomas. *J Neurooncol* 1987;5:277–285.
17. Ogawa T, Uemura K, Shishido F, et al. Changes of cerebral blood flow and oxygen and glucose metabolism following radiochemotherapy of gliomas: a PET study. *J Comput Assist Tomogr* 1988;12:290–297.
18. Ogawa T, Kanno I, Shishido F, et al. Clinical value of PET with ^{18}F-fluorodeoxyglucose and L-methyl-^{11}C-methionine for diagnosis of recurrent brain tumor and radiation injury. *Acta Radiol* 1991;32:197–202.
19. Patronas NJ, Di Chiro G, Kufta C, et al. Prediction of survival in glioma patients by means of positron emission tomography. *J Neurosurg* 1985;62:816–822.
20. Phelps ME, Huang SC, Hoffman EJ, Selin C, Sokoloff L, Kuhl DE. Tomographic measurement of local cerebral glucose metabolic rate in humans with (F-18)2-fluoro-2-deoxy-D-glucose: validation of method. *Ann Neurol* 1979;6:371–388.
21. Rozental JM, Levine RL, Nickles RJ. Changes in glucose uptake by malignant gliomas: preliminary study of prognostic significance. *J Neurooncol* 1991;10:75–83.
22. Herholz K, Rudolf J, Heiss WD. FDG transport and phosphorylation in human gliomas measured with dynamic PET. *J Neurooncol* 1992;12:159–165.
23. Herholz K, Ziffling P, Staffen W, et al. Uncoupling of hexose transport and phosphorylation in human gliomas demonstrated by PET. *Eur J Cancer Clin Oncol* 1988;24:1139–1150.
24. Sokoloff L. The deoxyglucose method: theory and practice. *Eur Neurol* 1981;20:137–145.
25. Reivich M, Alavi A, Wolf A, et al. Glucose metabolic rate kinetic model parameter determination in humans: the lumped constants and rate constants for [^{18}F]fluorodeoxyglucose and [^{11}C]deoxyglucose. *J Cereb Blood Flow Metab* 1985;5:179–192.
26. Kapoor R, Spence AM, Muzi M, Graham MM, Abbott GL, Krohn KA. Determination of the deoxyglucose and glucose phosphorylation ratio and the lumped constant in rat brain and a transplantable rat glioma. *J Neurochem* 1989;53:37–44.
27. Spence AM, Graham MM, Muzi M, et al. Deoxyglucose lumped constant estimated in a transplanted rat astrocytic glioma by the hexose utilization index. *J Cereb Blood Flow Metab* 1990;10:190–198.
28. Hamacher K, Coenen HH, Stocklin G. Efficient stereospecific synthesis of no-carrier-added 2-[^{18}F]-fluoro-2-deoxy-D-glucose using aminopolyether supported nucleophilic substitution. *J Nucl Med* 1986;27:235–238.
29. Shiue C-Y, Wolf AP. The synthesis of 1-[C-11]-D-glucose for measurement of brain glucose metabolism [Abstract]. *J Nucl Med* 1981;22:P58.

30. Shiue C-Y, Wolf AP. 1-11-C-D-glucose and related compounds, US Patent 4439414A, 1984.
31. Dence CS, Powers WJ, Welch MJ. Improved synthesis of 1-[^{11}C]D-glucose. *Appl Radiat Isot* 1993;44:971–980.
32. Lewellen TK, Bice AN, Harrison RL, Pencke MD, Link JM. Performance measurements of the SP-3000/UW time-of-flight emission tomograph. *IEEE Trans Nucl Sci* 1988;35:665–667.
33. Lewellen TK, Bice AN, Miyaoka RS, Harrison RL. Performance improvements for the SP-3000 time-of-flight positron emission tomograph [Abstract]. *J Nucl Med* 1990;31: 863.
34. Lewellen TK, Harrison RL, Bice AN. An experimental evaluation of the effect of time-of-flight information in image reconstructions for the Scanditronix/PETT electronics SP-3000 positron emission tomograph-preliminary results. *IEEE Trans Nucl Sci* 1989;36:1095–1099.
35. DeGrado TR, Turkington TG, Williams JJ, Stearns CW, Hoffman JM, Coleman RE. Performance characteristics of a whole-body PET scanner. *J Nucl Med* 1994;35:1398–1406.
36. Lewellen TK, Kohlmyer SG, Miyaoka RS, Kaplan MS, Stearns CW, Schubert SF. Investigation of the performance of the General Electric Advance positron emission tomograph in 3D mode. *IEEE Trans Nucl Sci* 1996;43:2199–2206.
37. Lewellen TK, Kohlmyer SG, Miyaoka RS, Schubert S, Stearns CW. Investigation of the count rate performance of General Electric Advance positron emission tomograph. *IEEE Trans Nucl Sci* 1995;42:1051–1057.
38. Graham MM, Lewellen BL. High-speed automated discrete blood sampling for positron emission tomography. *J Nucl Med* 1993;34:1357–1360.
39. Blomqvist G, Stone-Elander S, Halldin C, et al. Positron emission tomographic measurements of cerebral glucose utilization using [1–11-C]D-glucose. *J Cereb Blood Flow Metab* 1990;10:467–483.
40. Gjedde A, Diemer NH. Autoradiographic determination of regional brain glucose content. *J Cereb Blood Flow Metab* 1983;3:303–310.
41. Dennis JE, Gay DM, Welsch RE. An adaptive non-linear least squares algorithm. *ACM Trans Math Software* 1981;7:348–383.
42. Crane PD, Pardridge WM, Braun LD, Nyerges AM, Oldendorf WH. The interaction of transport and metabolism on brain glucose utilization: a reevaluation of the lumped constant. *J Neurochem* 1981;36:1601–1604.
43. Braun LD, Miller LP, Pardridge WM, Oldendorf WH. Kinetics of regional blood-brain barrier glucose transport and cerebral blood flow determined with the carotid injection technique in conscious rats. *J Neurochem* 1985;44:911–915.
44. Choi Y, Hawkins RA, Huang S-C, et al. Evaluation of the effect of glucose ingestion and kinetic model configurations of FDG in the normal liver. *J Nucl Med* 1994;35: 818–823.
45. Marshall RC, Huang SC, Nash WW, Phelps ME. Assessment of the [^{18}F]fluorodeoxyglucose kinetic model in calculations of myocardial glucose metabolism during ischemia. *J Nucl Med* 1983;24:1060–1064.
46. Suolinna EM, Haaparanta M, Paul R, Harkonen P, Solin O, Sipila H. Metabolism of 2-[^{18}F]fluoro-2-deoxyglucose in tumor-bearing rats: chromatographic and enzymatic studies. *Int J Radiat Appl Instrum B* 1986;13:577–581.
47. Wu HM, Huang SC, Choi Y, Hoh CK, Hawkins RA. A modeling method to improve quantitation of fluorodeoxyglucose uptake in heterogeneous tumor tissue. *J Nucl Med* 1995;36:297–306.
48. Herholz K, Wienhard K, Heiss WD. Validity of PET studies in brain tumors. *Cerebrovasc Brain Metab Rev* 1990;2:240–265.
49. Bass L, Bodsch W, Robinson PJ, Young MO. Metabolites of 2-deoxyglucose in rat brain at 12–24 h: bounds on kinetic constants. *Am J Physiol* 1987;253:E453–E460.
50. Haaparanta M, Paul R, Huovinen R, et al. Pharmacokinetics and metabolism of 2-[^{18}F]fluoro-2-deoxy-D-glucose (FDG) in mammary tumors of antiestrogen-treated rats. *Nucl Med Biol* 1995;22:483–489.
51. Nakada T, Kwee IL, Conboy CB. Noninvasive in vivo demonstration of 2-fluoro-2-deoxy-D-glucose metabolism beyond the hexokinase reaction in rat brain by ^{19}F nuclear magnetic resonance spectroscopy. *J Neurochem* 1986;46:198–201.
52. O'Connell TM, London RE. Identification of 2-fluoro-2-deoxy-D-glucose metabolites by 19F(1H) hetero-RELAY. *J Magn Resonance B* 1995;109:264–269.
53. Spence AM, Graham MM, Muzi M, et al. Feasibility of imaging pentose cycle glucose metabolism in gliomas with PET: studies in rat brain tumor models. *J Nucl Med* 1997;38:617–624.
54. Hawkins RA, Mans AM. Intermediary metabolism of carbohydrates and other fuels. In: Lajtha, A. eds. *Handbook of neurochemistry*, vol. 2. New York: Plenum Press; 1983:259–294.
55. Bassingthwaighte JB, Chan IS, Wang CY. Computationally efficient algorithms for convection-permeation-diffusion models for blood-tissue exchange. *Ann Biomed Eng* 1992;20:687–725.
56. Lear JL, Kasliwal RK. Autoradiographic measurement of cerebral lactate transport rate constants in normal and activated conditions. *J Cereb Blood Flow Metab* 1991;11: 576–580.
57. Floridi A, Paggi MG, Fanciulli M. Modulation of glycolysis in neuroepithelial tumors. *J Neurosurg Sci* 1989;33:55–64.
58. Oudard S, Poirson F, Miccoli L, et al. Mitochondria-bound hexokinase as target for therapy of malignant gliomas. *Int J Cancer* 1995;62:216–222.
59. Bennett MJ, Timperley WR, Taylor CB, Hill AS. Isoenzymes of hexokinase in the developing, normal and neoplastic human brain. *Eur J Cancer* 1978;14:189–193.
60. Katzen HM. The multiple forms of mammalian hexokinase and their significance to the action of insulin. *Adv Enzyme Regul* 1967;5:335–356.
61. Kurokawa M, Oda S, Tsubotani E, Fujiwara H, Yokoyama K, Ishibashi S. Characterization of hexokinase isoenzyme types I and II in ascites tumor cells by an interaction with mitochondrial membrane. *Mol Cell Biochem* 1982;45:151–157.
62. Sprengers ED, Koenderman AH, Staal GE. Mitochondrial and cytosolic hexokinase from rat brain: one and the same enzyme? *Biochim Biophys Acta* 1983;755:112–118.
63. Wilson JE. Brain hexokinase, the prototype ambiquitous enzyme. *Curr Top Cell Regul* 1980;16:1–54.
64. Eigenbrodt E, Fister P, Reinacher M. New perspectives on carbohydrate metabolism in tumor cells. In: Beitner, R. ed. *Regulation of carbohydrate metabolism*. Boca Raton: CRC Press; 1985:141–179.
65. Kraaijenhagen RJ, Rijksen G, Staal GE. Hexokinase isozyme distribution and regulatory properties in lymphoid cells. *Biochim Biophys Acta* 1980;631:402–411.
66. Oude Weernink PA, Rijksen G, Staal GE. Phosphorylation of pyruvate kinase and glycolytic metabolism in three human glioma cell lines. *Tumour Biol* 1991;12:339–352.
67. Singh M, Singh VN, August JT, Horecker BL. Transport and phosphorylation of hexoses in normal and Rous sarcoma virus-transformed chick embryo fibroblasts. *J Cell Physiol* 1978;97:285–292.
68. Cayanis E, Balinsky D. Comparative kinetic properties of human hexokinases. *Int J Biochem* 1975;6:741–749.
69. Grossbard L, Schimke RT. Multiple hexokinases of rat tissues. Purification and comparison of soluble forms. *J Biol Chem* 1966;241:3546–3560.
70. Katzen HM, Schimke RT. Multiple forms of hexokinase in the rat: tissue distribution, age dependency, and properties. *Proc Natl Acad Sci USA* 1965;54:1218–1225.
71. Ureta T. The comparative isozymology of vertebrate hexokinases. *Comp Biochem Physiol B* 1982;71:549–555.
72. Lusk JA, Manthorpe CM, Kao-Jen J, Wilson JE. Predominance of the cytoplasmic form of brain hexokinase in cultured astrocytes. *J Neurochem* 1980;34:1412–1420.
73. Hariharan R, Bray M, Ganim R, Doenst T, Goodwin GW, Taegtmeyer H. Fundamental limitations of [^{18}F]2-deoxy-2-fluoro-D-glucose for assessing myocardial glucose uptake. *Circulation* 1995;91:2435–2444.
74. Wienhard K, Pawlik G, Nebeling B, et al. Estimation of local cerebral glucose utilization by positron emission tomography: comparison of [^{18}F]2-fluoro-2-deoxy-D-glucose and [^{18}F]2-fluoro-2-deoxy-D-mannose in patients with focal brain lesions. *J Cereb Blood Flow Metab* 1991;11:485–491.
75. Lammertsma AA, Brooks DJ, Frackowiak RS, et al. Measurement of glucose utilization with [^{18}F]2-fluoro-2-deoxy-D-glucose: a comparison of different analytical methods. *J Cereb Blood Flow Metab* 1987;7:161–172.
76. American Academy of Neurology, Therapeutics, and Technology Assessment Subcommittee Assessment. Positron emission tomography. *Neurology* 1991;41:163–167.
77. Hanson MW, Glantz MJ, Hoffman JM, et al. FDG-PET in the selection of brain lesions for biopsy. *J Comput Assist Tomogr* 1991;15:796–801.
78. Theodore WH. Antiepileptic drugs and cerebral glucose metabolism. *Epilepsia* 1988;29(suppl 2):S48–S55.
79. Fiorelli M, Blin J, Bakchine S, Laplane D, Baron JC. PET studies of cortical diaschisis in patients with motor hemi-neglect. *J Neurol Sci* 1991;104:135–142.
80. Kushner M, Alavi A, Reivich M, Dann R, Burke A, Robinson G. Contralateral cerebellar hypometabolism following cerebral insult: a positron emission tomographic study. *Ann Neurol* 1984;15:425–434.
81. Kushner M, Tobin M, Alavi A, et al. Cerebellar glucose consumption in normal and pathologic states using fluorine-FDG and PET. *J Nucl Med* 1987;28:1667–1670.
82. Rozental JM, Levine RL, Nickles RJ, Dobkin JA, Hanson JM. Cerebral diaschisis in patients with malignant glioma. *J Neurooncol* 1990;8:153–161.
83. Di Chiro G, Brooks RA. PET quantitation: blessing and curse. *J Nucl Med* 1988;29:1603–1604.